Science Advances
AAAS

Supplementary Materials for

Identification of the active triple-phase boundary of a non-Pt catalyst layer in fuel cells

Yu-Cheng Wang *et al.*

Corresponding author: Yu-Cheng Wang, wangyc@xmu.edu.cn; Shu-Hui Sun, shuhui.sun@inrs.ca; Zhi-You Zhou, zhouzy@xmu.edu.cn

Sci. Adv. **8**, eadd8873 (2022)
DOI: 10.1126/sciadv.add8873

This PDF file includes:

Figs. S1 to S32
Tables S1 to S5

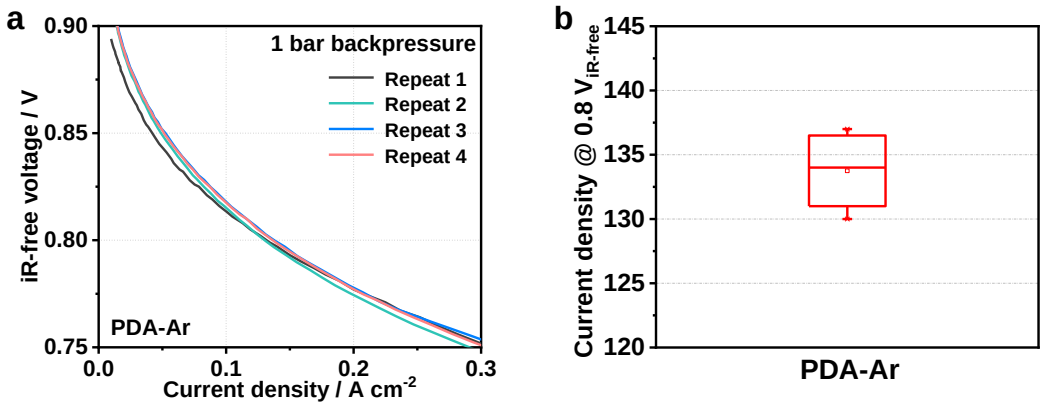

Fig. S1. Polarization curves of PDA-Ar cathode. (a) Four-times repeated polarization curves (iR-free) and (b) error bar of H_2-O_2 PEMFC test in ethanol solvent. Testing conditions: 80 °C (cell temperature); back pressure = 1 bar; flow rate = 0.3 slpm with 100 % RH; N212 membrane; cathode catalyst = PDA-Ar (4.0 mg cm^{-2}); anode catalyst = Pt/C (40 wt%, JM) with 0.4 mg_{pt} cm^{-2}.

Fig. S1 shows that polarization curves of H_2-O_2 PEMFC exhibit good reproducibility with the current density of 130~137 mA cm^{-2} at 0.8 $V_{iR\text{-}free}$.

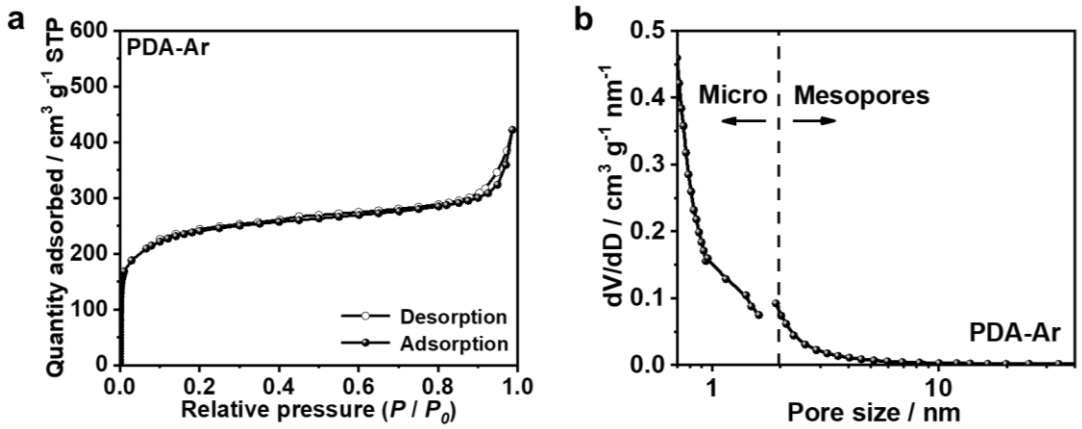

Fig. S2. Surface area and pore size distribution of PDA-Ar catalyst. (a) Ar adsorption/desorption isotherms of PDA-Ar catalyst and (b) micropore (HK method) and mesopore (BJH method) size distributions of PDA-Ar catalyst.

The PDA-Ar shows a type-I isotherm with a large adsorption capacity in the low-pressure region, implying a typical microporous material.

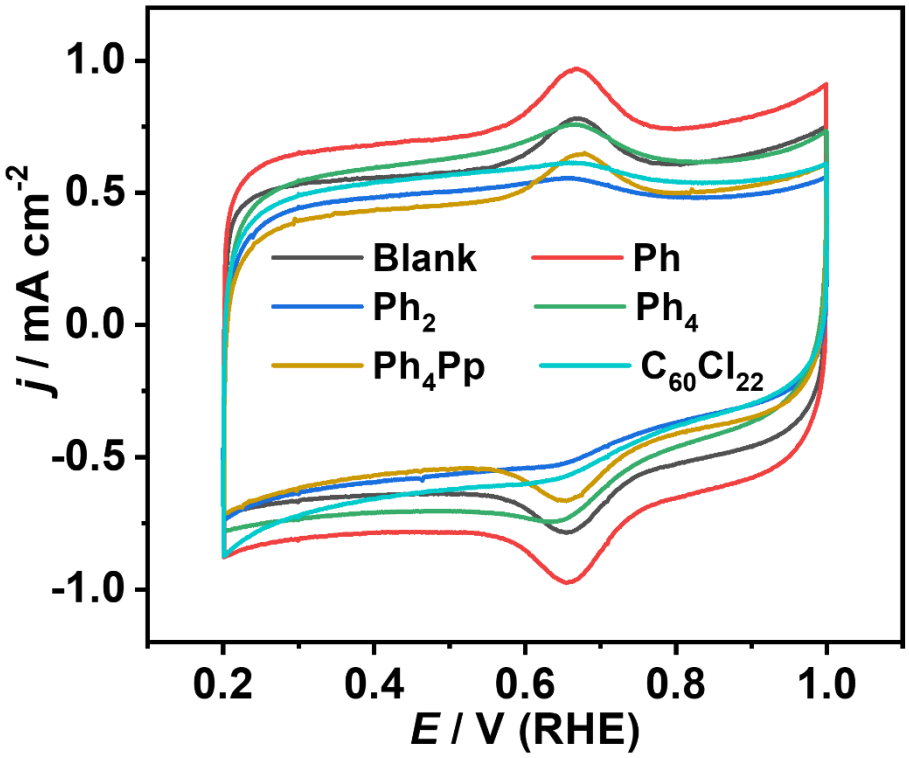

Fig. S3. CV background curves before and after organics addition. Cyclic voltammetry (CV) background curves of PDA-Ar catalyst before and after the addition of organics (Ph, Ph_2, Ph_4, Ph_4Pp, and $C_{60}Cl_{22}$). Test conditions: in Ar-saturated 0.1 M H_2SO_4 solution, at 0.6 mg cm^{-2} of catalyst loading, at 10 mV s^{-1} between 0.2 V and 1.0 V (RHE), at 30 °C water bath.

No new peak is observed in the background CV curves after the addition of organics, demonstrating the electrochemical inertness of these organics.

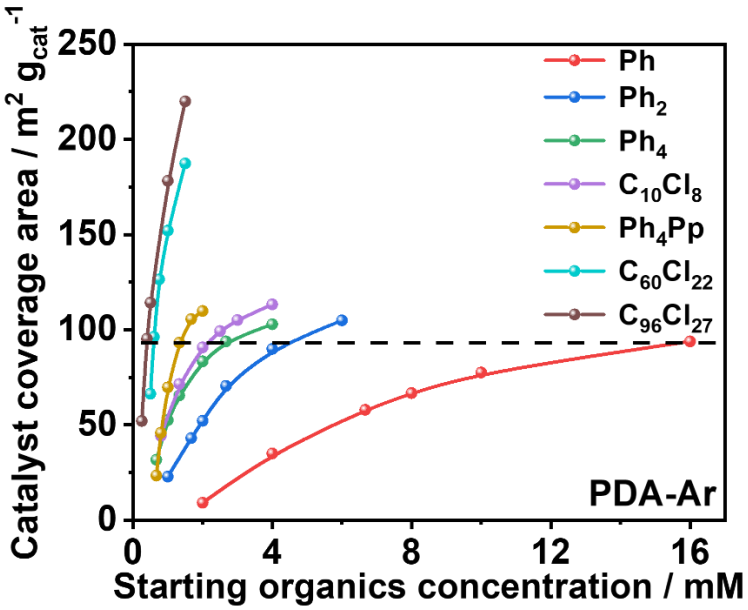

Fig. S4. Catalyst surface coverage. The plot of catalyst coverage area versus starting organics concentration for the PDA-Ar catalyst.

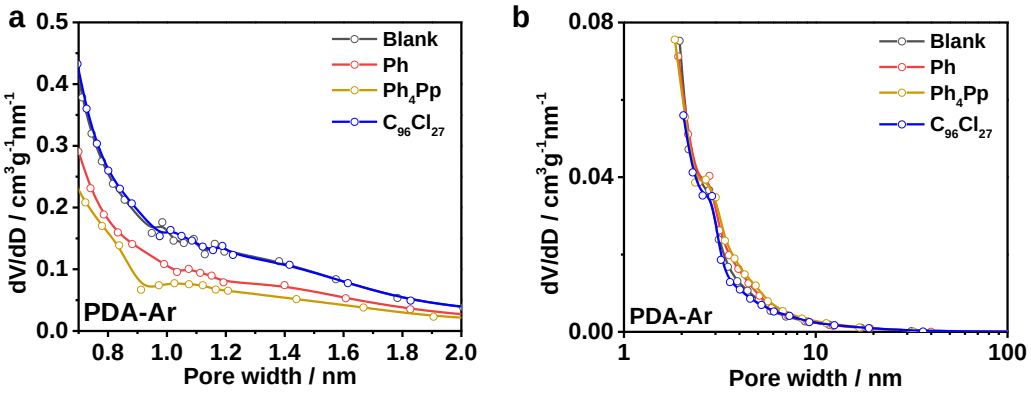

Fig. S5. Impact of organics addition on micropore accessibility. (a) Micropore (HK method) and (b) mesopore (BJH method) size distributions of PDA-Ar catalyst with and without the addition of organics. i.e., Ph, Ph_4Pp, and $C_{96}Cl_{27}$.

Both the Ph and Ph_4Pp decreased the micropore accessibility while impacting little on the mesopore or macropore region. The larger Ph_4Pp blocked more micropore than the smaller Ph even at the same catalyst surface coverage. By contrast, the largest $C_{96}Cl_{27}$ was mainly absorbed by the external surfaces and impacted little on the micropore accessibility. This experimental observation is in good agreement with the assumption of size-selective pore blockage.

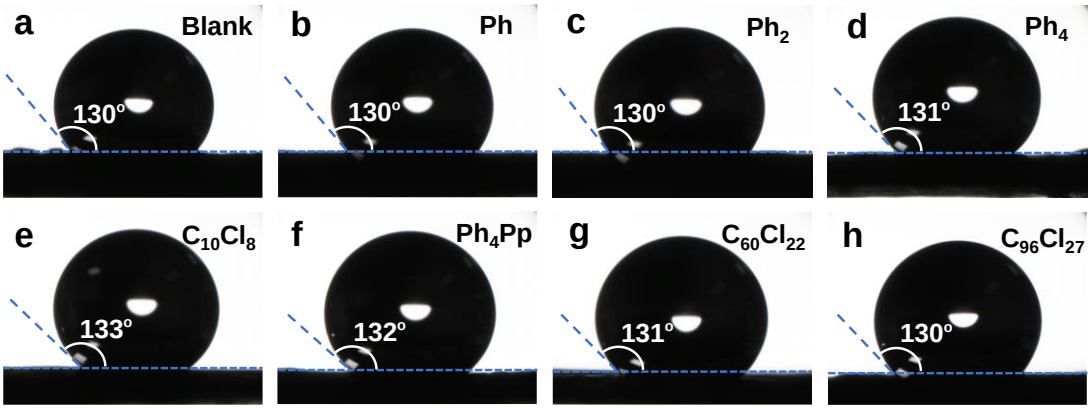

Fig. S6. Impact of organics addition on surface wettability. Comparison of surface wettability of the cathodes. (a) the bare PDA-Ar cathode; (b-h) with the addition of organics, i.e., Ph, Ph_2, Ph_4, $C_{10}C_8$, Ph_4Pp, $C_{60}Cl_{22}$, and $C_{96}Cl_{27}$.

After the addition of different-sized organics, the surface contact angle varied between 130 and 133° with less 2% of the variation.

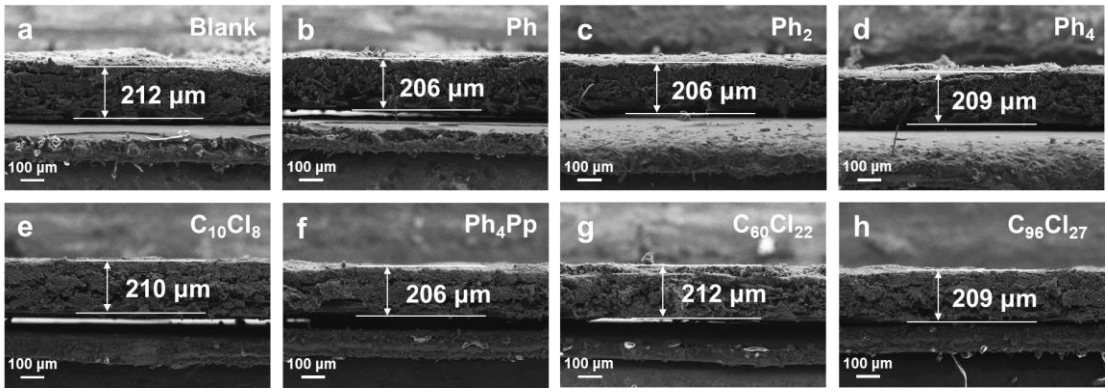

Fig. S7. Impact of organics addition on cathode thickness. SEM images of the cross-section of the cathodes. (a) the bare PDA-Ar cathode; (b-h) with the addition of organics, i.e., Ph, Ph_2, Ph_4, $C_{10}C_8$, Ph_4Pp, $C_{60}Cl_{22}$, and $C_{96}Cl_{27}$.

Below 2% of the variation in the catalyst layer thickness was observed after the seven probe molecules were added.

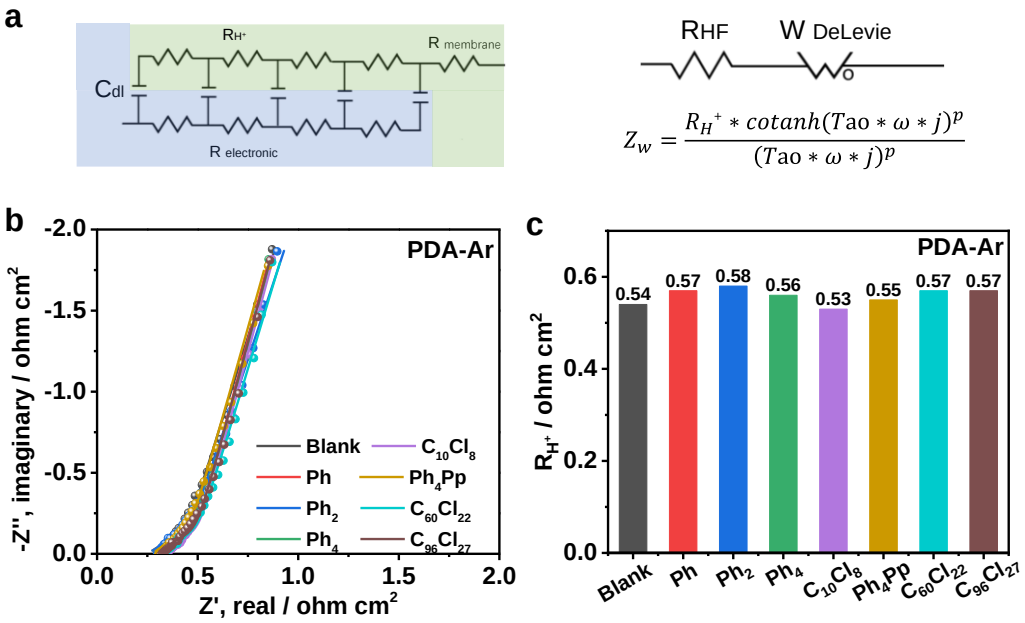

Fig. S8. Impact of organics addition on proton transport. (a) Transmission line circuit represents the electronic and ionic components of the porous electrode and the ionic membrane in a nitrogen atmosphere. C_{dl} is double-layer capacitance; R_{H+} is the proton transport resistance of electrodes; $R_{membrane}$ is ionic resistance of Nafion membrane; $R_{electronic}$ is the electrical resistance. (b) The equivalent circuit used for analyzing EIS. R_{HF} is high-frequency (HF) cell resistance, equal to the sum of $R_{membrane}$ and $R_{electronic}$; $W_{De\ Levie}$ is the Warburg impedance, contributed by R_{H+} and C_{dl}. The cotanh function is used for fitting Warburg impedance. τ is the time constant ($\tau = R_{H+}{*}C_{dl}$); ω is the frequency, and p is the exponent. (c) EIS spectrum and fitting result based on the transmission line model. (d) Comparison of R_{H+} of the MEA with and without the addition of organics.

The R_{H+} of bare MEA was 0.54 Ω cm^2. After the addition of different-sized organics, the R_{H+} varied between 0.53 and 0.58 Ω cm^2 with less 5% of the variation.

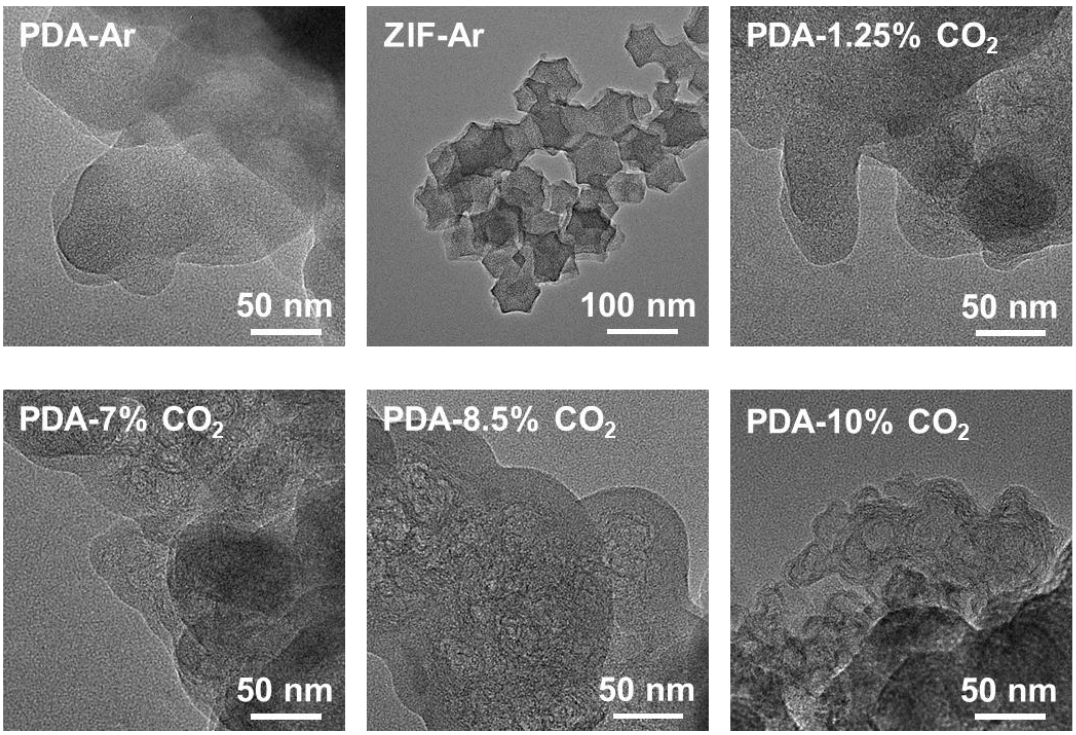

Fig. S9. Catalyst morphology. TEM images of six Fe/N/C catalysts.

The five PDA-series catalysts show a similar carbon morphology and consist of roughly 100 nm aggregated particles, which is different from the ZIF-Ar catalyst consisting of polyhedral carbon structures.

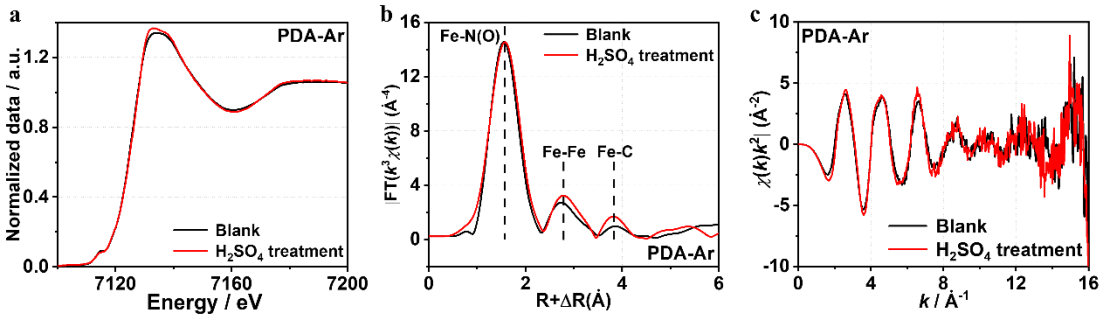

Fig. S10. XAS measurement. (a) Normalized Fe K-edge XANES spectra, (b) Fourier-transformed EXAFS data, and (c) k^3-weighted FT-EXAFS spectra of PDA-Ar catalyst before and after H_2SO_4 treatment.

The prominent peak at 1.56 Å plus a small peak at 2.6 Å confirms the Fe species mainly in the atomically dispersed form. After H_2SO_4 treatment, no apparent change is found in the XANES and k^3-weighted FT-EXAFS spectra, suggesting that acid treatment has little impact on the coordination structure of Fe-N_x active sites in the PDA-Ar catalyst.

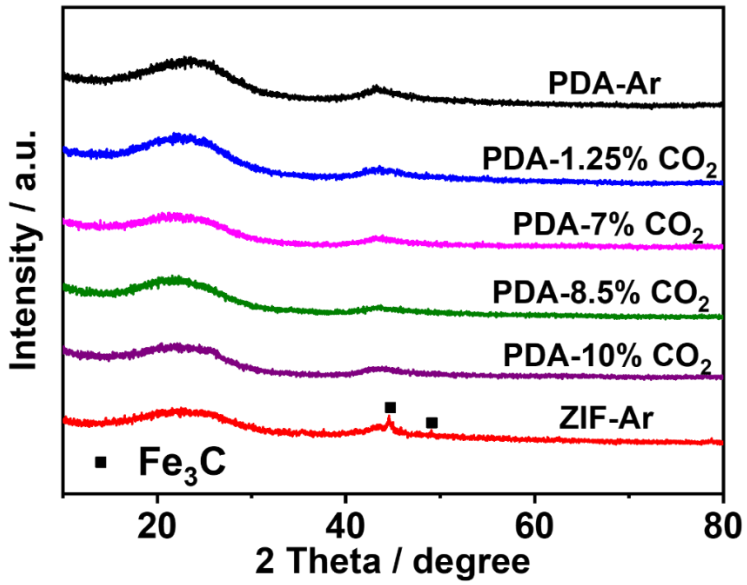

Fig. S11. XRD measurement. XRD patterns of six Fe/N/C catalysts.

No observable Fe crystalline peaks are observed in the five PDA-series Fe/N/C catalysts. The peaks observed in the ZIF-Ar are assigned to Fe_3C nanoparticles (PDF#35-0772).

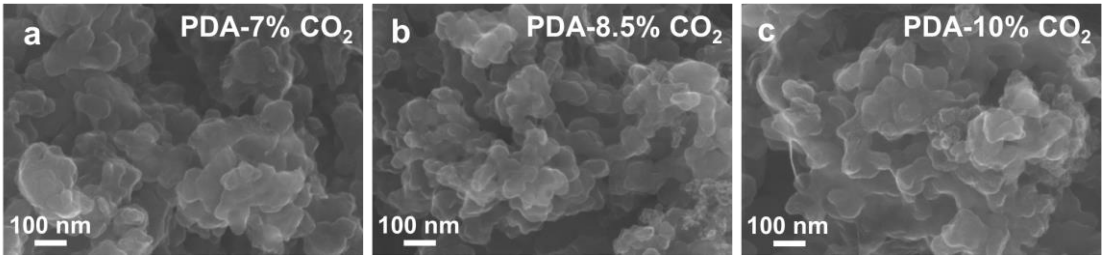

Fig. S12. Catalyst surface morphology. SEM images of three PDA-series Fe/N/C catalysts. (a) PDA-7% CO_2; (b) PDA-8.5% CO_2 and (c) PDA-10% CO_2.

The three catalysts show a similar carbon morphology.

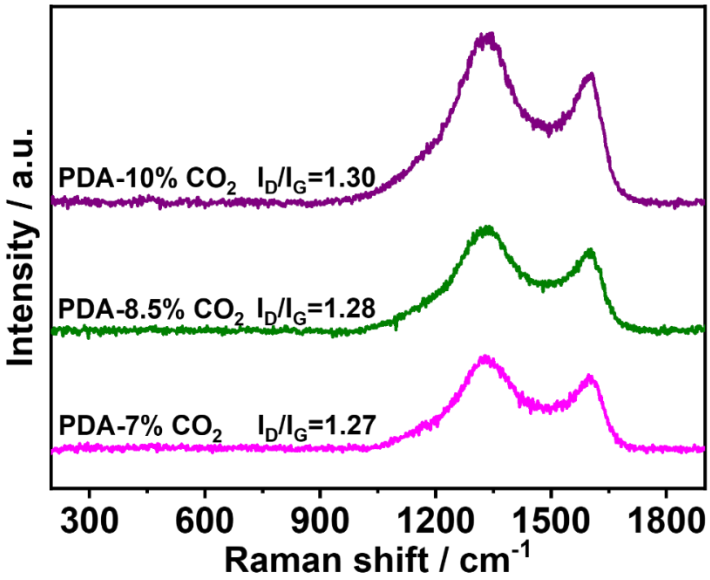

Fig. S13. Raman spectra measurement. Raman spectra of three PDA-series Fe/N/C catalysts. i.e., PDA-7% CO_2, PDA-8.5% CO_2 and PDA-10% CO_2.

The nearly-identical I_D/I_G values support a similar degree of carbon defect.

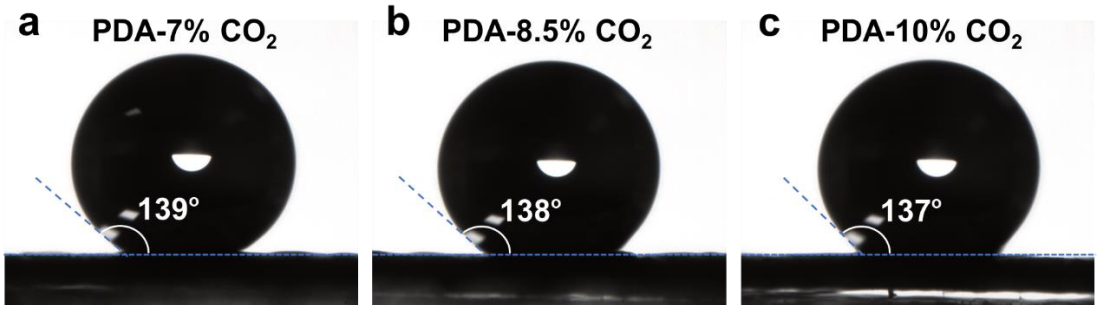

Fig. S14. Contact angle measurement. Comparison of surface wettability of three different Fe/N/C cathodes. (a) PDA-7% CO_2; (b) PDA-8.5% CO_2 and (c) PDA-10% CO_2.

The nearly-identical contact angle supports a similar surface wettability of the cathodes.

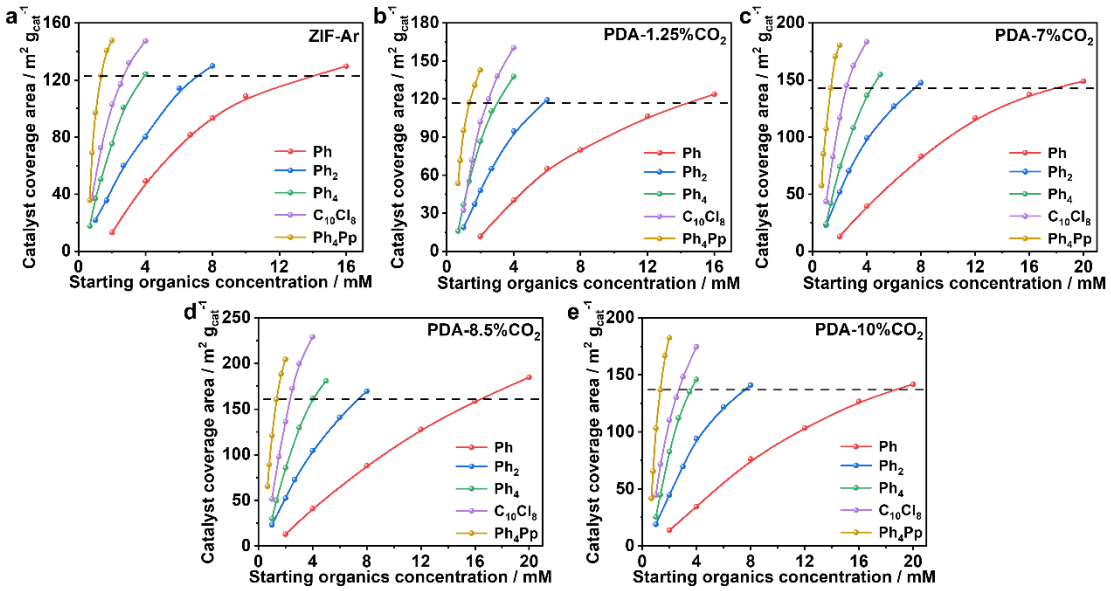

Fig. S15. Catalyst surface coverage after organics addition. The plot of catalyst coverage area versus starting organics concentration for the five Fe/N/C catalysts. (a) ZIF-Ar; (b) PDA-1.25% CO_2; (c) PDA-7% CO_2;(d) PDA-8.5% CO_2; (e) PDA-10% CO_2.

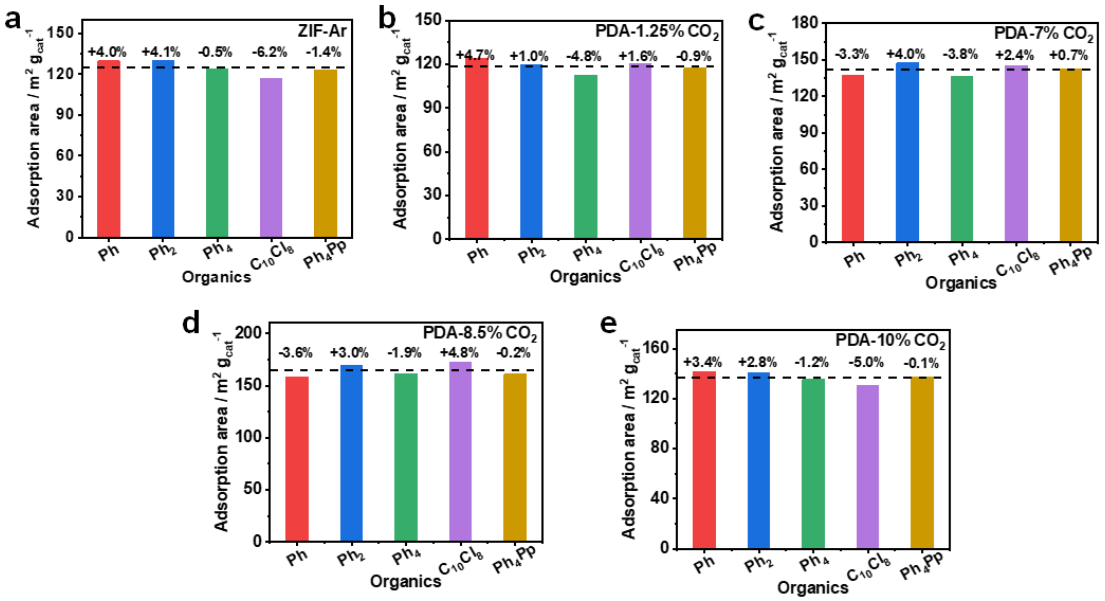

Fig. S16. Controlled catalyst surface coverage. Controlled coverage area of the catalyst by five different organics for the fuel cell activity test. (a) ZIF-Ar; (b) PDA-1.25% CO_2; (c) PDA-7% CO_2;(d) PDA-8.5% CO_2; (e) PDA-10% CO_2.

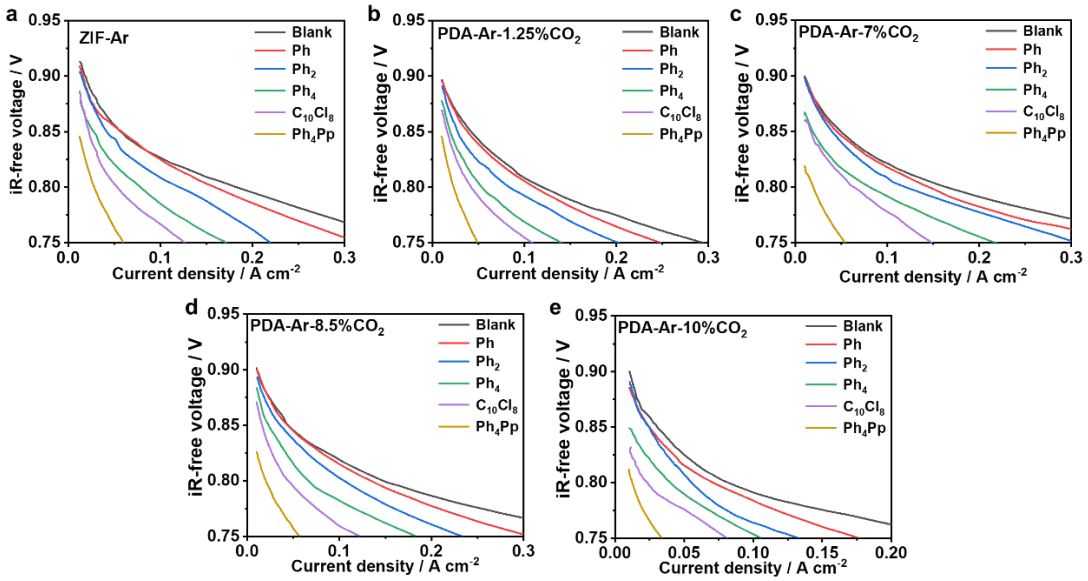

Fig. S17. Impact of organics addition on fuel cell performance. Polarization curves (iR-free) of H_2-O_2 PEMFC test with and without the addition of different-sized organics (Ph, Ph_2, Ph_4, $C_{10}Cl_8$ and Ph_4Pp) using (a) ZIF-Ar, (b) PDA-1.25% CO_2, (c) PDA-7% CO_2, (d) PDA-8.5% CO_2 and (e) PDA-10% CO_2 as the cathode catalyst, respectively. Test conditions: cell temperature = 80 °C; back pressure = 1 bar; flow rate = 0.3 slpm with 100 % RH; N212 membrane; cathode catalyst loading = 4.0 mg cm^{-2}; anode catalyst = Pt/C (40 wt%, JM) with 0.4 mg_{pt} cm^{-2}.

The six Fe/N/C catalysts possess different pore structures. However, they show a similar molecular size-dependent activity change trend.

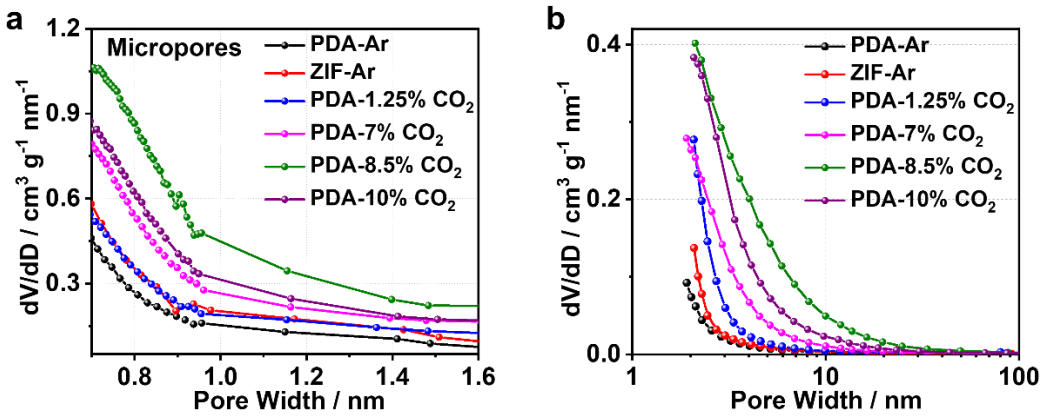

Fig. S18. Pore size distributions. (a) Micropore (HK method) and (b) mesopore (BJH method) size distributions of PDA-Ar, ZIF-Ar, PDA-1.25% CO_2, PDA-7% CO_2, PDA-8.5% CO_2, and PDA-10% CO_2 catalysts, respectively.

CO_2 can etch the carbon to create more pores during the high-temperature treatment. Both micropores and mesopores volume increased after the CO_2 etching (0% to 8.5%). However, at a higher CO_2 content, i.e., 10%, both the micropores and mesopores volume started to decline, which can be attributed to the over-etching of CO_2 under high temperature.

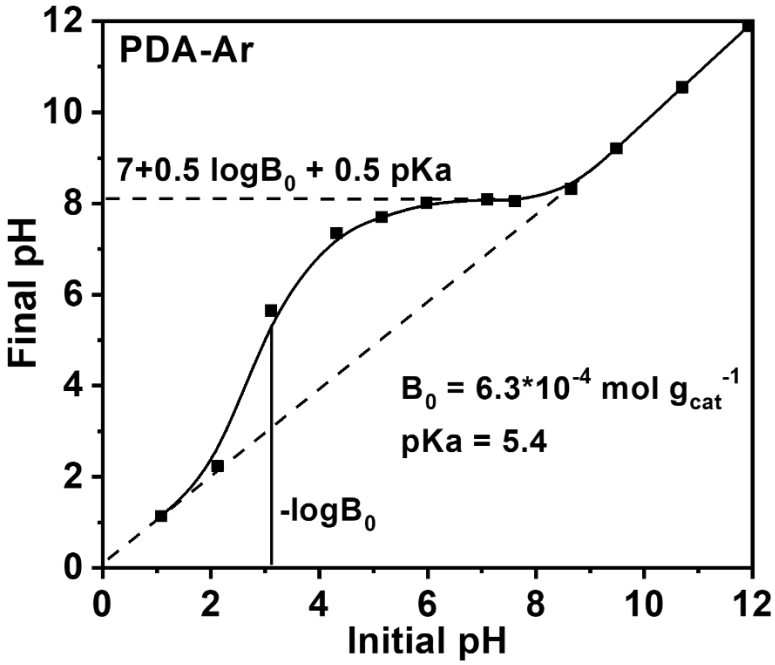

Fig. S19. Surface pK_a and functional groups. The plot of pH values in the solution after the acid-alkaline titration *versus* the initial given pH values. Titration conditions: 20 mg of PDA-Ar catalyst was immersed in 10 mL of aqueous solution with a given pH ranging from 1 to 12, then the final pH was measured.

According to the fitting curve, the concentration of basic groups (B_0) and pK_a on the surface of PDA-Ar catalyst is calculated to be 6.3 $\times 10^{-4}$ mol g_{cat}^{-1} and 5.4, respectively. The rationality of such estimation is illustrated in a previous reported work by Juan Herranz et al. *(43)*

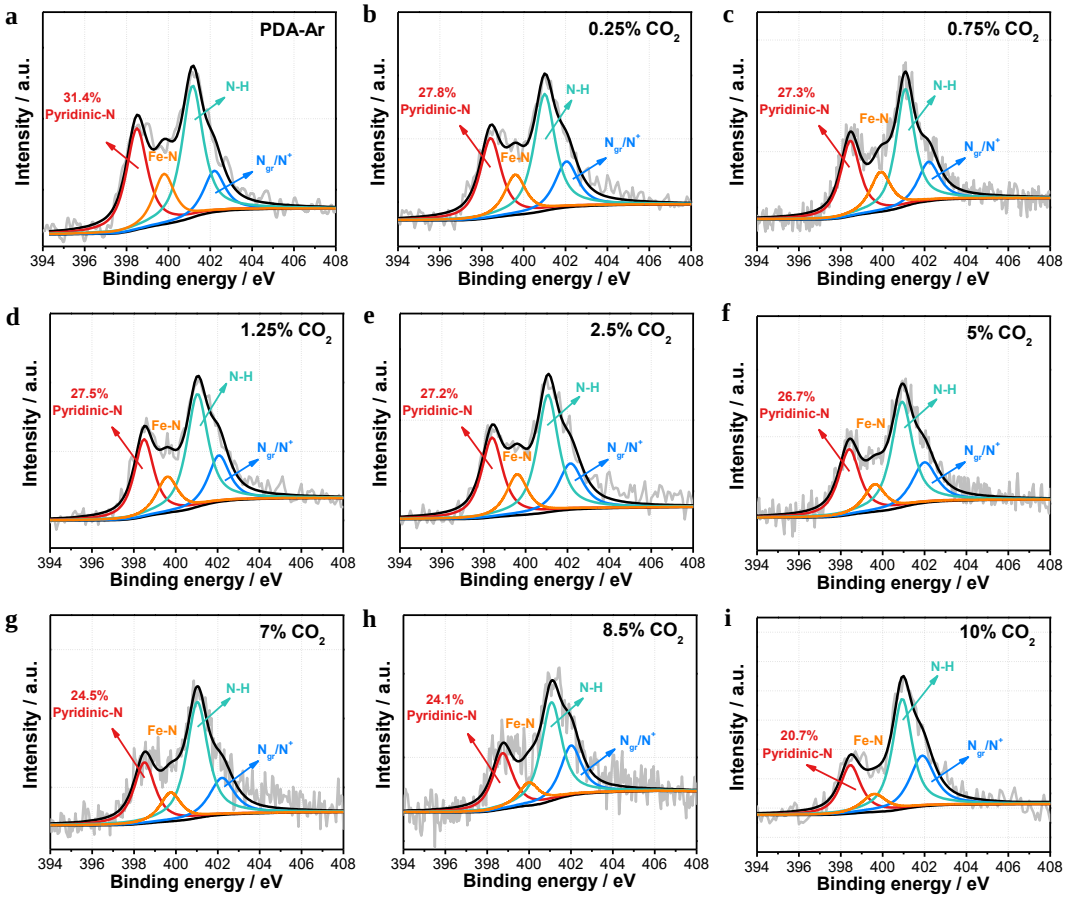

Fig. S20a. XPS without Nafion. High-resolution N1s XPS spectra and the corresponding peak deconvolution of nine different Fe/N/C catalysts. The fitting parameters are listed in Table S4A. The deviation of FWHM for each peak is below than 10%.

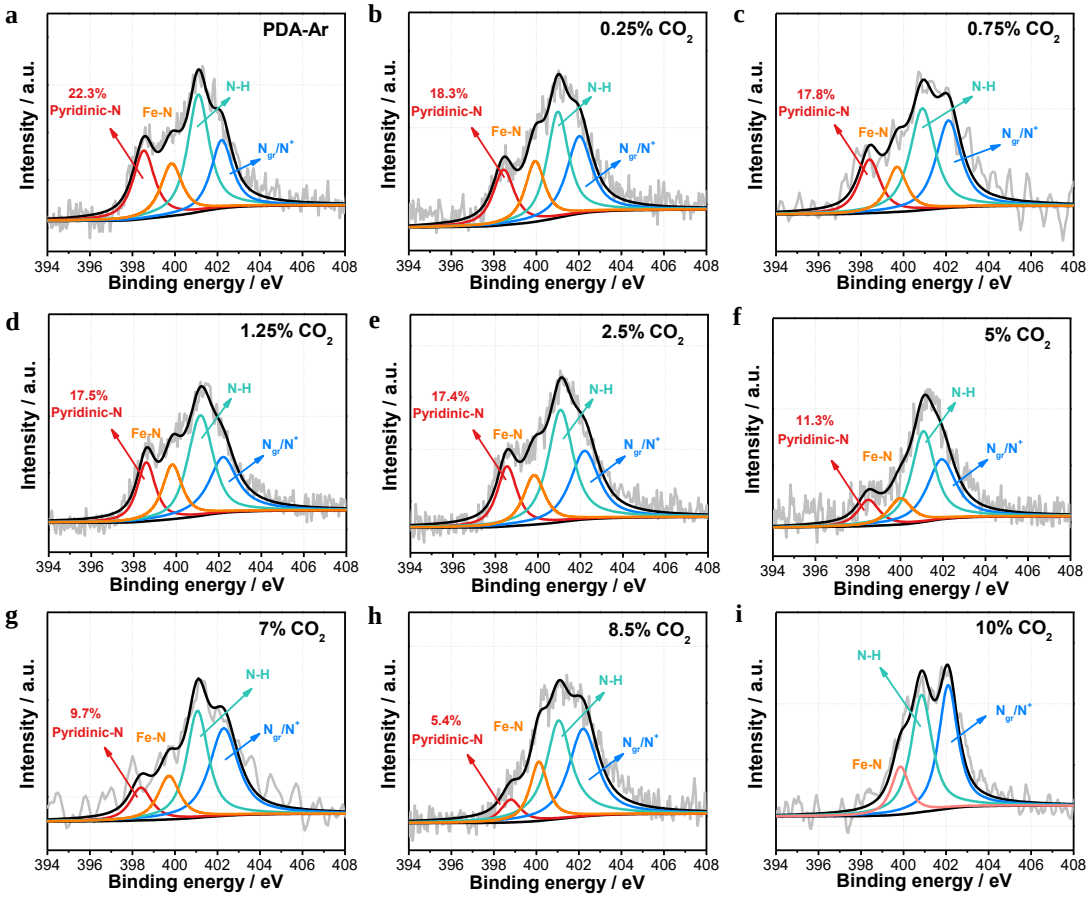

Fig. S20b. XPS with Nafion. High-resolution N1s XPS spectra and the corresponding peak deconvolution of nine different Fe/N/C catalysts after mixing with Nafion. The mass ratio of catalyst to Nafion was 1:1.3. The fitting parameters are listed in Table S4B. The deviation of FWHM for each peak is controlled below than 10%.

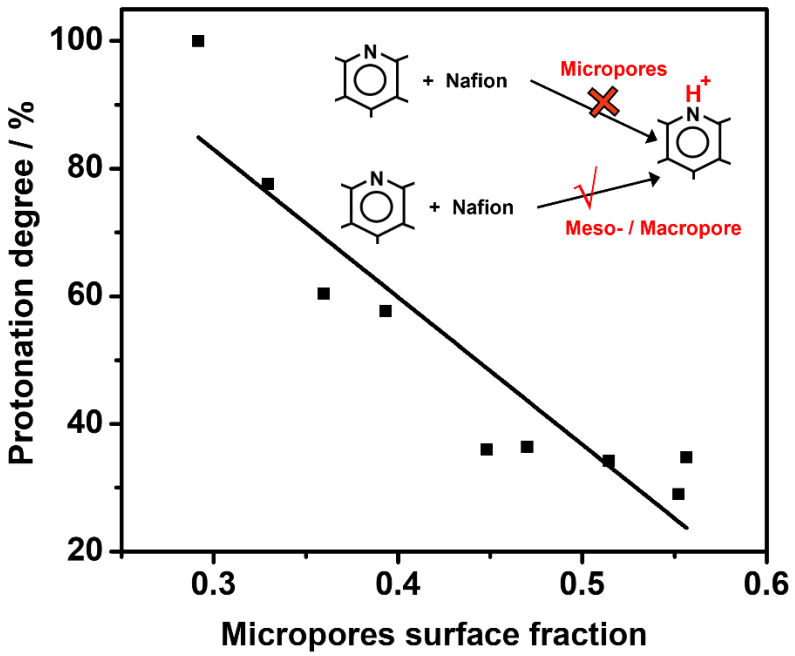

Fig. S20c. Micropore fraction versus protonation degree. The plot of protonation degree of pyridinic-N on the surface of Fe/N/C catalysts *versus* their micropores surface fraction.

The micropores surface fraction of Fe/N/C catalyst is represented by the ratio of micropores surface area to BET surface area. The protonation degree of pyridinic-N was calculated according to the following formula: $(1 - N_{after}/N_{before}) \times 100\%$, here N_{before} and N_{after} are the content of pyridinic-N of the catalyst before and after mixing with Nafion, respectively. As shown in **Fig. S20c**, a negative correlation of protonation degree of pyridinic-N to micropores surface fraction is established, indicating that acidic Nafion can hardly neutralize basic pyridinic-N species in micropores, but it can proronate pyridinic-N in larger mesopores or macropores.

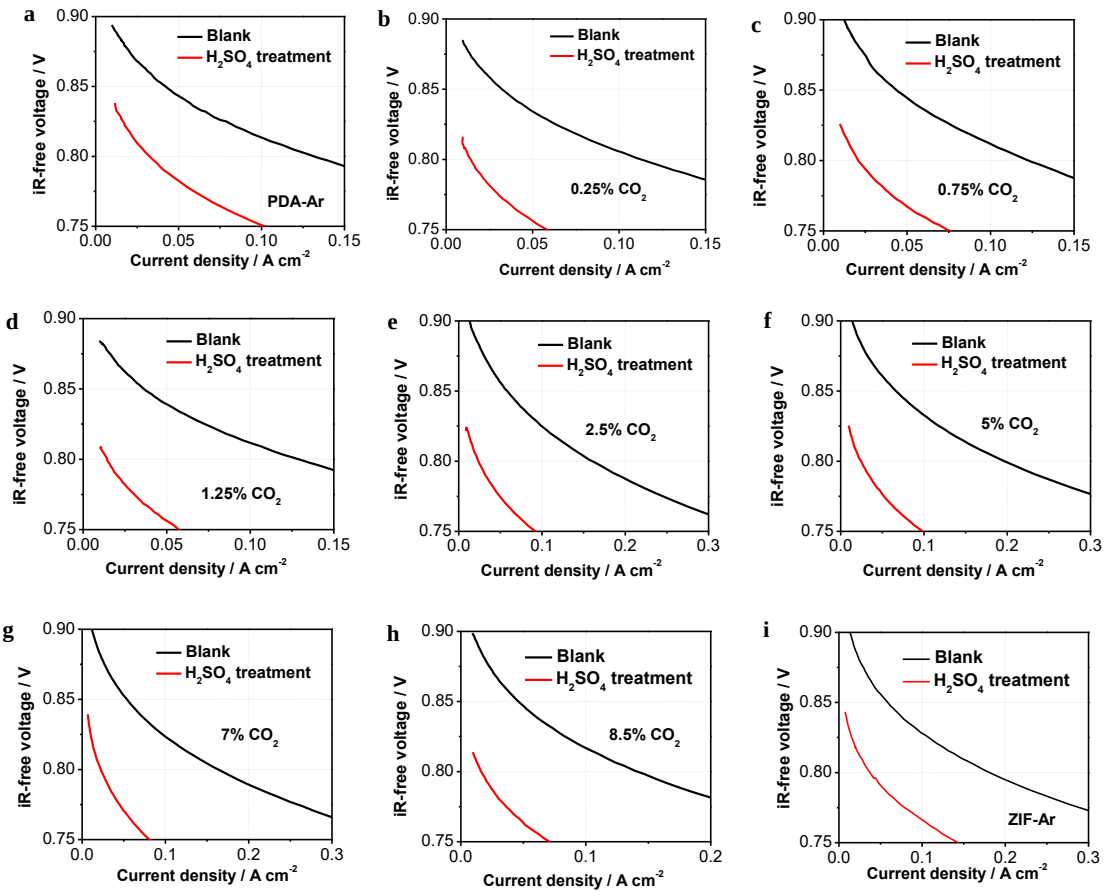

Fig. S21. Impact of acid treatment on fuel cell performance. Polarization curves (iR-free) of H_2-O_2 PEMFC testing with and without the addition of H_2SO_4 using nine different Fe/N/C catalysts as the cathode, respectively. Test conditions: cell temperature = 80 °C; back pressure = 1 bar; flow rate = 0.3 slpm with 100 % RH; N212 membrane; cathode catalyst loading = 4.0 mg cm^{-2}; anode catalyst = Pt/C (40 wt%, JM) with 0.4 mg_{pt} cm^{-2}, H_2SO_4 concentration = 1.0 $\boldsymbol{\mu mol\ mg_{cat}^{-1}}$. The treatment process was as follows: Fe/N/C catalyst was dispersed in ethanol, followed by the addition of H_2SO_4 solution with stirring for 1h. Then, Nafion solution (5 wt%) was added to form the cathode ink. The blank Fe/N/C cathode was prepared similarly except for the addition of H_2SO_4 in the ink preparation process.

H_2SO_4 treatment results in 75-89% of current density loss at 0.8 $V_{iR\text{-}free}$ for nine Fe/N/C catalysts.

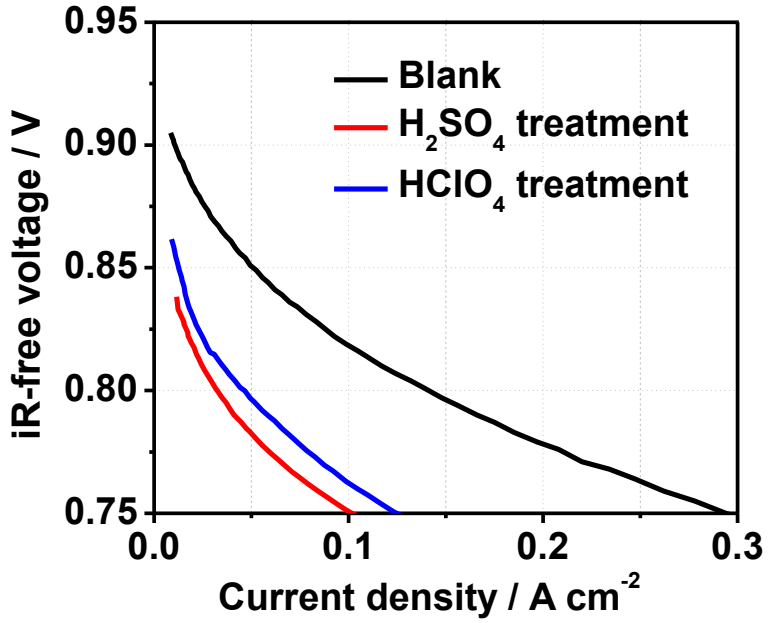

Fig. S22. ORR activity before and after acid treatment. Polarization curves (iR-free) of H_2-O_2 PEMFC using PDA-Ar as the cathode catalyst with and without acid (H_2SO_4 and $HClO_4$) treatment. Test conditions: 80 °C (cell temperature); back pressure = 1 bar; flow rate = 0.3 slpm with 100 % RH; N212 membrane; cathode catalyst loading = 4.0 mg cm^{-2}; anode catalyst = Pt/C (40 wt%, JM) with 0.4 mg_{pt} cm^{-2}, H_2SO_4 or $HClO_4$ concentration 1.0 $\boldsymbol{\mu mol\ mg_{cat}^{-1}}$.

H_2SO_4 and $HClO_4$ treatment results in 80% and 70% of current density loss at 0.8 $V_{iR\text{-}free}$, respectively, suggesting that the deactivation effect of acids on Fe/N/C catalyst results from the H^+ instead of the specific adsorption of SO_4^{2-} on active sites.

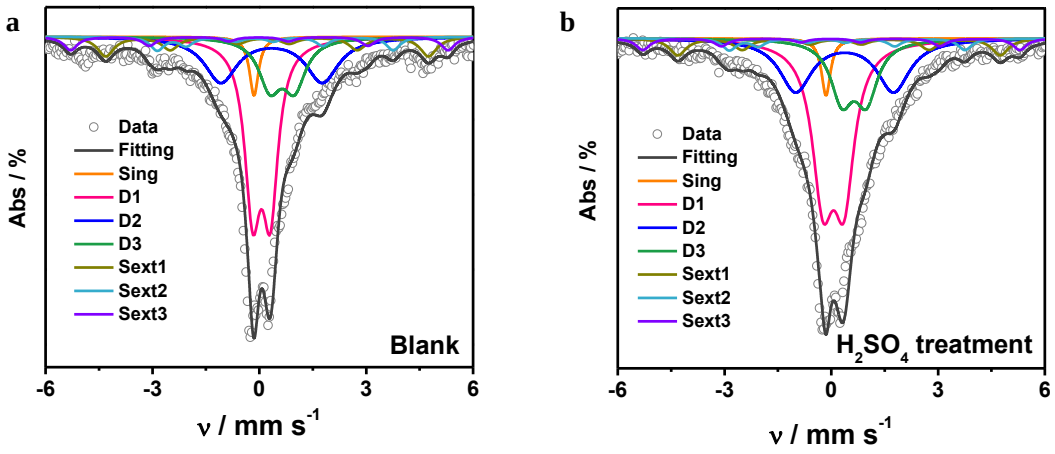

Fig. S23. Mössbauer spectrum before and after acid treatment. ^{57}Fe Mössbauer transmission spectrum and their fittings with seven spectral components for PDA-Ar catalyst before (a) and after (b) H_2SO_4 treatment. The fitting parameters were listed in Table S4.

The Mössbauer spectrum is fitted with one singlet, three doublets (D1, D2 and D3), and three sextets (Sext1, Sext2, Sext3). The three sextets and the singlet are attributed to be inorganic Fe-species, such as α-iron and/or iron carbide. The doublets D1, D2 and D3 are assigned to square-planar Fe(II)N_4 coordination with Fe(II) in a low-, intermediate -, and high-spin state, respectively. After acid leaching, the content of the singlet and three sextets decreases by 26% and 47−50%, respectively (**Table S5C**). This result suggests that a portion of inorganic Fe species are removed by acid leaching. However, the content of ORR-related species, like the three doublets, decreases by only 5.1−8.5%, suggesting that acid treatment has little impact on the number of Fe-N_x active sites.

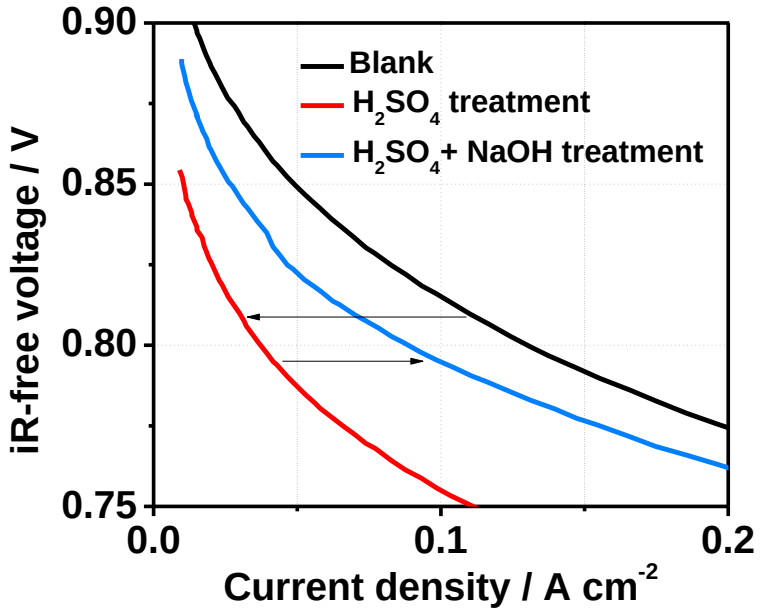

Fig. S24. Catalyst activity recovery. Alkaline treatment to recover the activity of acid-treated PDA-Ar catalyst.

Acid treatment decreases the current density from 130 to 35 mA cm^{-2} at 0.8 $V_{iR\text{-}free}$. After alkaline treatment, the current density recovers to 80 mA cm^{-2} at 0.8 $V_{iR\text{-}free}$, reaching 60% of the initial activity.

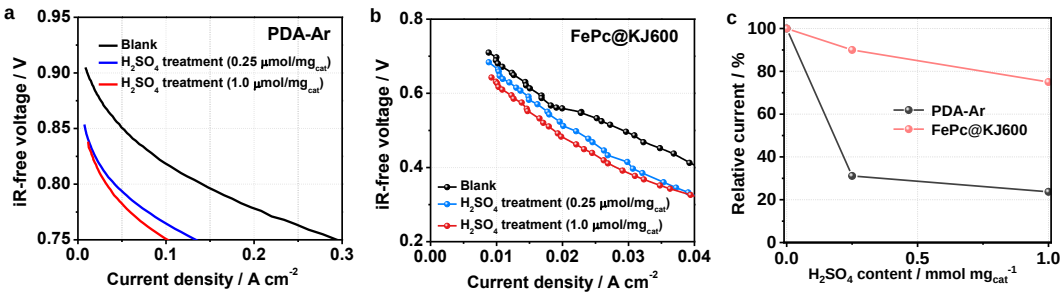

Fig. S25. Impact of acid treatment on fuel cell performance. The response of PDA-Ar and FePC@KJ600 catalysts toward H_2SO_4. (a) Polarization curves (iR-free) of H_2-O_2 PEMFC test with PDA-Ar as the cathode catalyst with and without H_2SO_4 treatment. (b) Polarization curves (iR-free) of H_2-O_2 PEMFC test with FePc@KJ600 as the cathode catalyst with and without H_2SO_4 treatment. (c) The relative variation in ORR activity with increasing H_2SO_4 concentration during the post-treatment process.

In the case of PDA-Ar catalyst, H_2SO_4 treatment results in 75% of current density loss at 0.8 $V_{iR\text{-}free}$ upon addition of 1.0 $\mu mol\, mg_{cat}^{-1}$ H_2SO_4. By contrast, FePc@KJ600 catalyst without pyridinic-N exhibits only 24% activity loss after H_2SO_4 treatment. This difference suggests that pyridinic-N is sensitive to acids, the protonation of pyridinic-N decreases the catalytic activity of adjacent Fe-N_x sites.

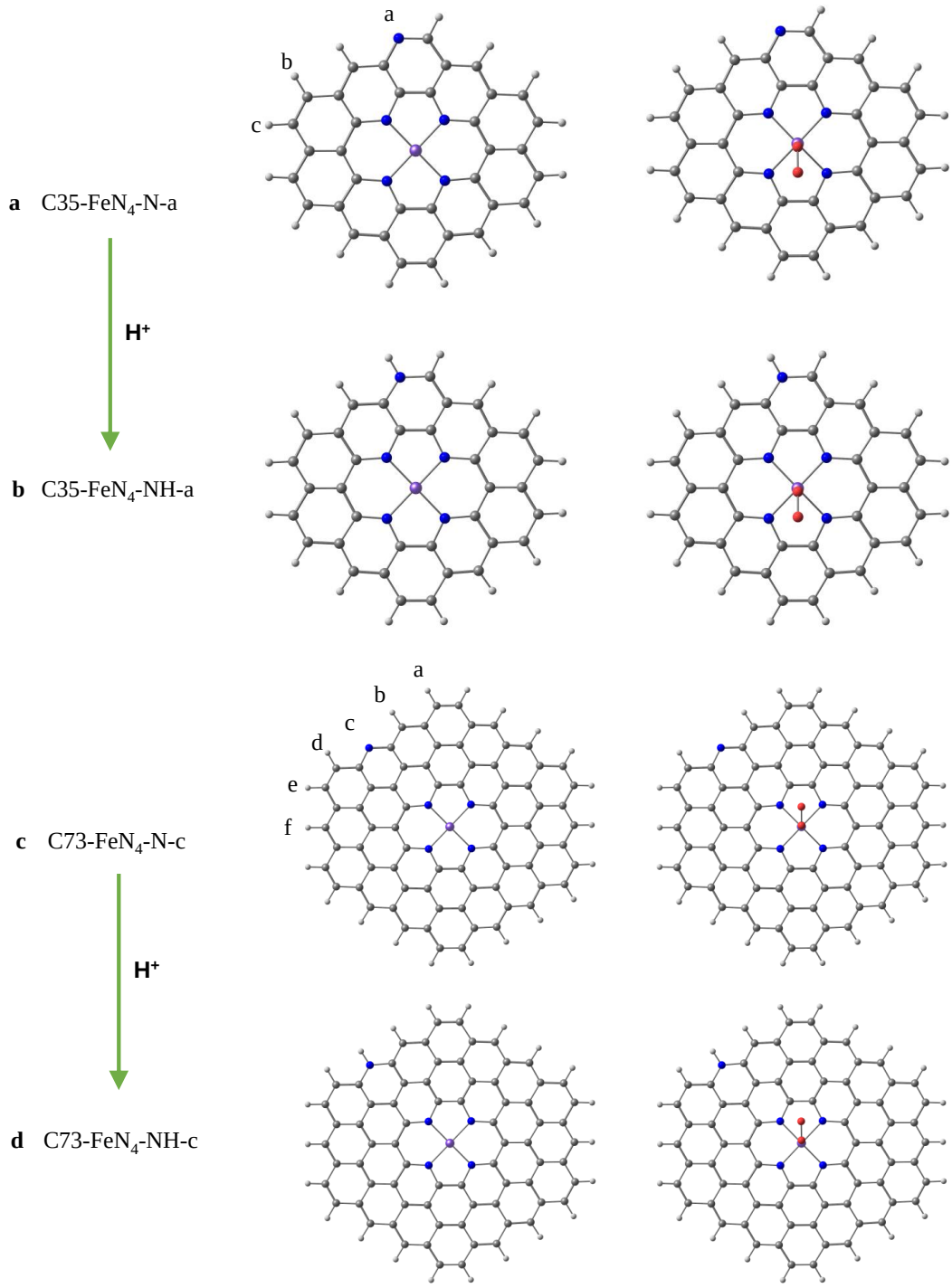

Fig. S26. Structures for theoretical calculation. Top views of the C35-FeN_4-N-a and C73-FeN_4-N-c structures and their corresponding O_2 adsorption configurations before and after protonation. These structures are derived according to the position of N-pyridine. The other relevant structures have the same Fe-N-C molecular frame but different N sites along the molecule edge.

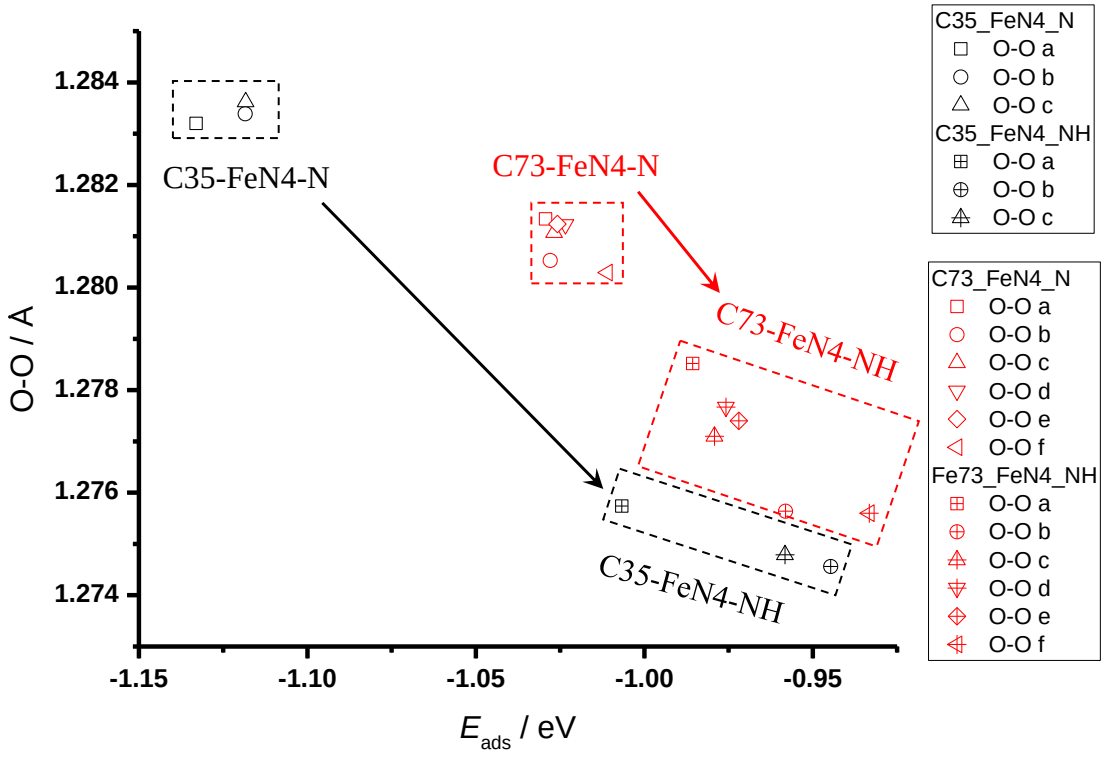

Fig. S27. O-O bond length versus adsorption energy. Plots of O-O bond length versus O_2 adsorption energy at the C35-FeN_4-N and the C73-FeN_4-N structures before and after the protonation of pyridinic-N.

It can be found out that there is a correlation between O_2 adsorption energy and its O-O bond length on the FeN_4 molecular structures. After the protonation of N-pyridine at the molecule edge, O_2 adsorption at the Fe center is weakened. Correspondingly, the O-O bond length is shorter than that sample without the pyridinic-N protonation. This trend can take effect on both of C35-FeN_4-N and C73-FeN_4-N structures.

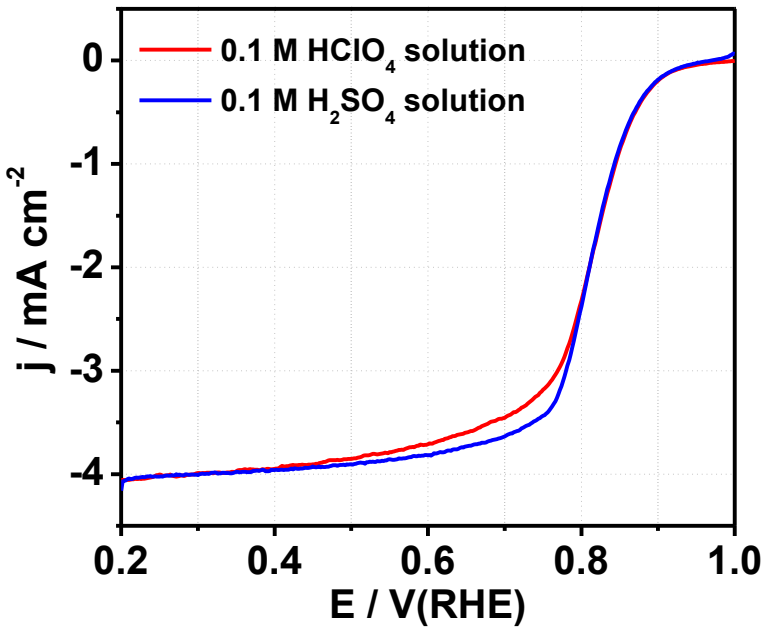

Fig. S28. ORR activity tested in different electrolytes. ORR polarization curves of PDA-Ar catalyst using 0.1 M H_2SO_4 and $HClO_4$ solution as the electrolyte, respectively.

The PDA-Ar catalyst shows the same high ORR activity by RDE test in different electrolytes.

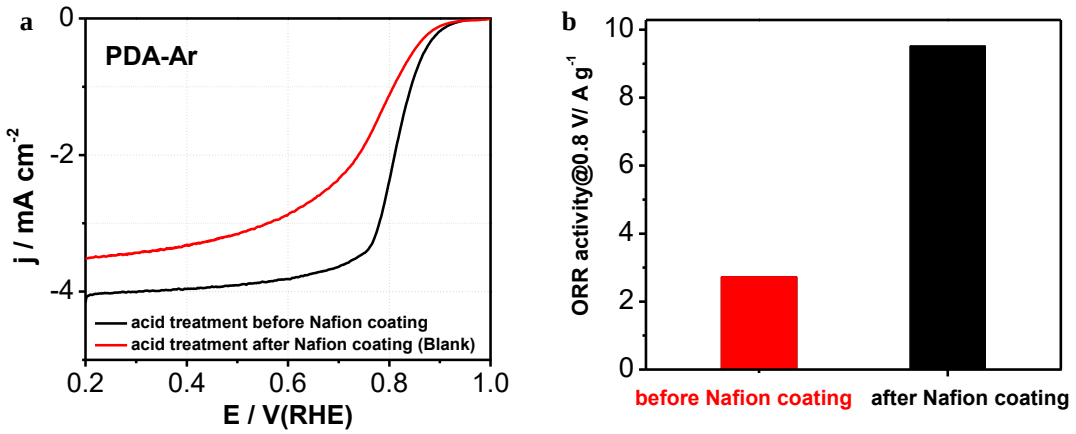

Fig. S29. Impact of acid treatment on ORR activity at different stages. (a) ORR polarization curves of PDA-Ar catalyst by RDE test after different acid treatment processes. Red curve: Acid treatment was conducted prior to Nafion coating. Black curve: Acid treatment was conducted after Nafion coating. (b) Comparison of ORR mass activity of Fe/N/C catalyst at 0.8 V_{RHE}.

We observe that mass activity of the catalyst decreases by 72% at 0.8 V_{RHE} if H_2SO_4 treatment conducted before the coating of Nafion, suggesting that Nafion coating on Fe/N/C catalyst can prevent the protonation of pyridinic-N species, ensuring the high ORR activity.

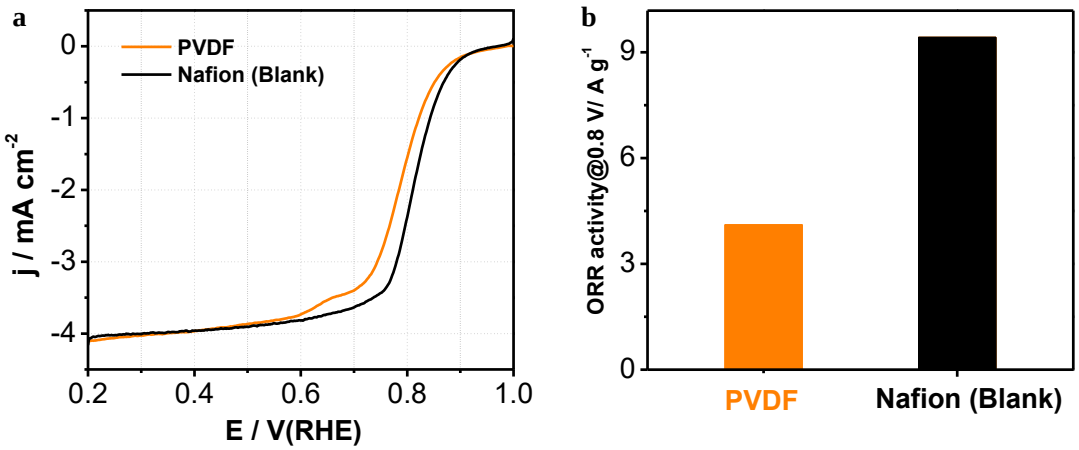

Fig. S30. ORR activity tested with different binders. (a) ORR polarization curves of PDA-Ar catalyst by RDE test using PVDF and PTFE as the binder, respectively, in O_2-saturated 0.1 M H_2SO_4 solution. (b) Comparison of ORR mass activity of Fe/N/C catalyst at 0.8 V_{RHE}.

The replacement of Nafion by PVDF as the binder decreases the mass activity by 60% at 0.8 V_{RHE}, suggesting the rapid activity loss of PDA-Ar catalyst in 0.1 M H_2SO_4 solution in the case of PVDF binder.

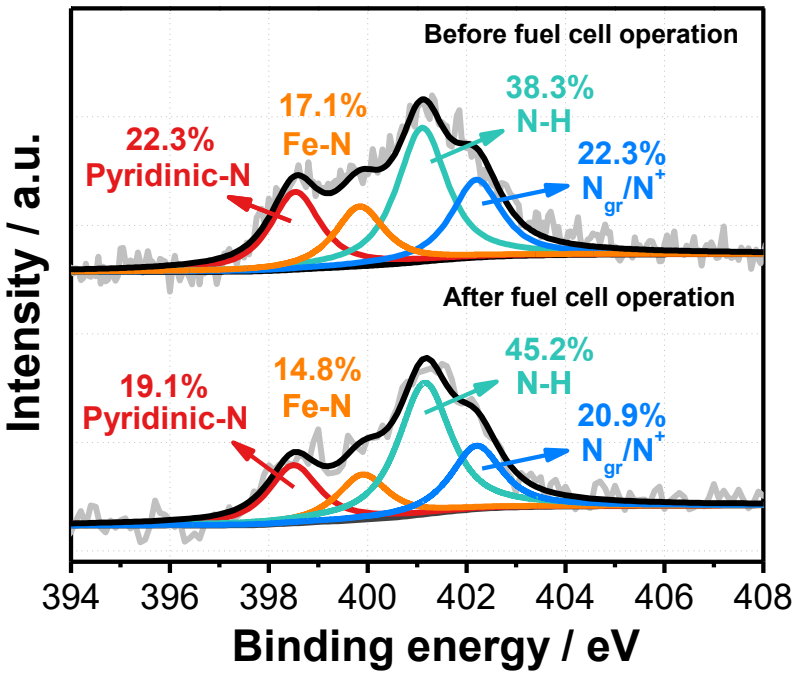

Fig. S31. XPS spectra before and after fuel cell operation. High-resolution N1s XPS spectra and the corresponding peak deconvolution of PDA-Ar catalyst before and after fuel cell operation. Fuel cell operation conditions: five cycles of polarization curve test from OCP to 0.25 V.

After fuel cell operation, the content of pyridinic-N shows a negligible decrease from 22.3% to 19.1%.

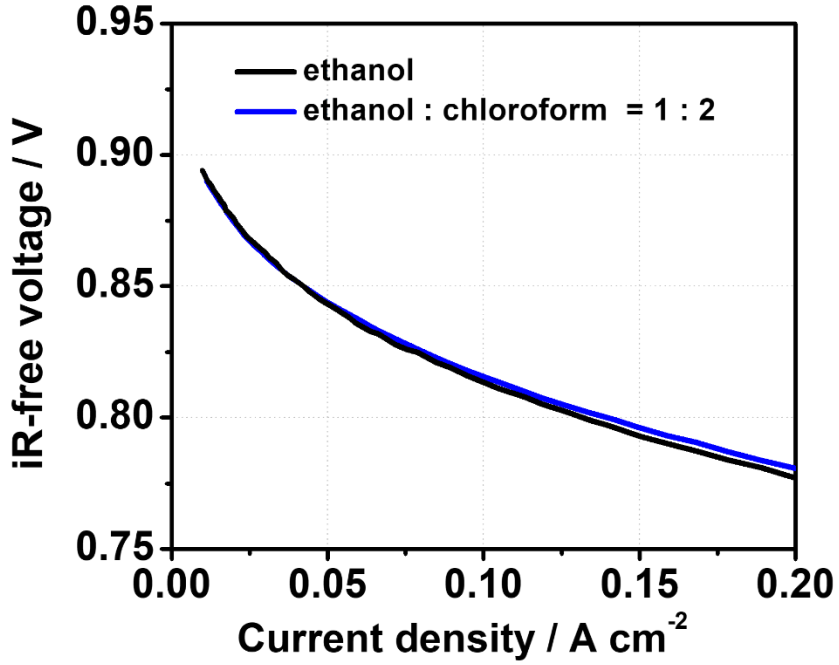

Fig. S32. Fuel cell performance using different solvents. Polarization curves (iR-free) of H_2-O_2 PEMFC using different solvents in the ink fabrication process. Testing conditions: 80 °C (cell temperature); back pressure = 1 bar; flow rate = 0.3 slpm with 100 % RH; N212 membrane; cathode catalyst = PDA-Ar (4.0 mg cm^{-2}); anode catalyst = Pt/C (40 wt%, JM) with 0.4 mg_{pt} cm^{-2}.

Fig. S32 shows only 7% of performance variation at 0.8 $V_{iR\text{-}free}$ using two different solvents in the ink fabrication process, suggesting a negligible effect of solvents on ORR performance.

Table S1.

Summary of dynamic diameter of different organic compounds and the corresponding pore size that can be blocked.

Organics	Dynamic diameter (d_1)	O_2 dynamic diameter (d_2)	Pore size ($d_p = d_1 + d_2$)
Ph	0.5219 nm	0.3467 nm	0.8686 nm ≈ 0.8 nm[a]
Ph_2	0.6693 nm		1.016 nm ≈ 1.0 nm
Ph_4	0.8943 nm		1.241 nm ≈ 1.2 nm
$C_{10}Cl_8$	1.1931 nm		1.539 nm ≈ 1.5 nm
Ph_4Pp	1.6733 nm		2.020 nm ≈ 2.0 nm
$C_{60}Cl_{22}$	2.0855 nm		2.432 nm ≈ 2.4 nm
$C_{96}Cl_{27}H_3$	2.6179 nm		3.020 nm ≈ 3.1 nm[a]

a. The approximation of the boundary size gives a looser pore size range.

Table S2.

Summary of BET surface area, micropores surface area and external surface area of six different Fe/N/C catalysts.

Catalyst	BET surface area ($m^2 g^{-1}$)	Micropores surface area ($m^2 g^{-1}$)	External surface area ($m^2 g^{-1}$)
PDA-Ar	756.31	417.62	338.69
ZIF-Ar	922.09	615.25	376.84
PDA-1.25%-CO_2	1054.89	495.87	559.02
PDA-7%-CO_2	1228.18	441.72	786.46
PDA-8.5%-CO_2	1576.32	519.16	1057.16
PDA-10%-CO_2	1258.12	366.87	891.25

Table S3.

Summary of Fe element content of the six Fe/N/C catalysts determined by ICP-MS.

Smaple	Fe content (wt%)
PDA-Ar	0.78
PDA-1.25% CO_2	0.59
PDA-7% CO_2	0.40
PDA-8.5% CO_2	0.35
PDA-10% CO_2	0.29
ZIF-Ar	4.22

Table S4A.

Corresponding fitting parameters of XPS peaks of nine different Fe/N/C catalysts before mixing with Nafion.

Catalyst	Py-N			Fe-N			Pr-N/N-H			Gr-N		
	Position	Area	FWHM	Position	Area	FWHM	Position	Area	FWHM	Position	Area	FWHM
0%-CO_2	398.5	2516.08	1.2	399.8	1251.48	1.2	401.15	3273.25	1.2	402.2	1025.09	1.2
0.25%-CO_2	398.5	2223.30	1.2	399.6	1128.58	1.2	401.1	3252.95	1.2	402.1	1386.34	1.3
0.75%-CO_2	398.5	2213.07	1.11	399.9	1257.17	1.2	401.1	3233.58	1.05	402.2	1243.50	1.2
1.25%-CO_2	398.5	1835.22	1.11	399.6	928.45	1.2	401.05	2890.67	1.2	402.1	1190.68	1.2
2.5%-CO_2	398.4	1982.22	1.2	399.6	1023.87	1.2	401.1	2916.97	1.2	402.15	1338.33	1.3
5%-CO_2	398.4	1727.79	1.2	399.6	723.00	1.2	401.0	2772.74	1.2	402.0	1242.29	1.3
7%-CO_2	398.5	1563.27	1.2	399.75	736.09	1.2	401.0	2967.13	1.2	402.2	1102.21	1.3
8.5%-CO_2	398.7	1140.98	1.16	399.9	520.63	1.2	401.1	2022.51	1.17	402.0	1051.80	1.2
10%-CO_2	398.5	28.52	1.17	399.6	12.72	1.3	401.0	61.95	1.12	401.9	35.59	1.3

Table S4B.

Corresponding fitting parameters of XPS peaks of nine different Fe/N/C catalysts after mixing with Nafion.

Catalyst	Py-N			Fe-N			Pr-N/N-H			Gr-N/N^+		
	Position	Area	FWHM	Position	Area	FWHM	Position	Area	FWHM	Position	Area	FWHM
0%-CO_2	398.5	2532.70	1.2	399.85	1947.18	1.2	401.1	4356.17	1.2	402.2	2526.12	1.2
0.25%-CO_2	398.5	1270.67	1.2	399.9	1280.22	1.1	401.1	2434.05	1.2	402.0	2081.54	1.3
0.75%-CO_2	398.4	1196.58	1.2	399.7	927.44	1.1	401.1	2644.24	1.3	402.1	2273.75	1.3
1.25%-CO_2	398.6	1553.50	1.01	399.8	1563.83	1.1	401.15	3398.05	1.2	402.2	2474.30	1.3
2.5%-CO_2	398.5	1900.34	1.11	399.8	1689.53	1.2	401.1	4461.42	1.2	402.2	3124.54	1.3
5%-CO_2	398.5	816.82	1.2	399.9	886.62	1.2	401.1	3062.41	1.2	402.0	2495.60	1.3
7%-CO_2	398.4	501.25	1.2	399.7	650.69	1.2	401.05	2383.62	1.3	402.2	1684.27	1.3
8.5%-CO_2	398.8	656.89	1.11	400.0	1537.42	1.1	401.05	3823.24	1.2	402.2	3648.42	1.3
10%-CO_2	-	-	-	399.85	1155.52	1.05	401.0	3337.65	1.12	402.1	3206.74	1.1

Table S5A.

Average Mössbauer parameters derived from the fitting curves data of PDA-Ar catalyst before acid leaching. Isomer shift (IS), quadrupole splitting (QS), line width (LW), and relative spectral area (%) of each component.

Before acid leaching	IS ($mm \cdot s^{-1}$)	QS ($mm \cdot s^{-1}$)	LW ($mm \cdot s^{-1}$)	Area (%)
S1	-0.15	--	0.30	3.78
D1	0.06	0.49	0.50	36.13
D2	0.34	2.84	1.10	19.44
D3	0.64	0.68	0.75	15.19
SIX1	0.17	0.09	0.56	11.33
SIX2	0.15	0.58	0.46	7.05
SIX3	-0.01	0.02	0.46	7.05

Table S5B.

Average Mössbauer parameters derived from the fitting curves data of PDA-Ar catalyst after acid leaching. Isomer shift (IS), quadrupole splitting (QS), line width (LW), and relative spectral area (%) of each component.

After acid leaching	IS ($mm \cdot s^{-1}$)	QS ($mm \cdot s^{-1}$)	LW ($mm \cdot s^{-1}$)	Area (%)
S1	-0.15	--	0.30	3.44
D1	0.06	0.58	0.71	40.71
D2	0.37	2.75	1.10	22.70
D3	0.64	0.68	0.75	17.17
SIX1	0.17	0.09	0.56	7.42
SIX2	0.15	0.58	0.46	4.27
SIX3	-0.01	0.02	0.46	4.27

Table S5C.

Comparison of Fe content of each component before and after acid leaching.

Fe content（wt%）	Before acid leaching	After acid leaching	Relative variation
S1	0.0060	0.0045	26%
D1	0.0578	0.0529	8.4%
D2	0.0311	0.0295	5.1%
D3	0.0243	0.0223	8.5%
SIX1	0.0181	0.0096	47%
SIX2	0.0113	0.0054	52%
SIX3	0.0113	0.0054	52%
Total content	0.16	0.13	81%

Fe content of PDA-Ar catalyst before and after acid leaching was determined by ICP-MS.